


Article

Tribo-Surface Variation Caused by Ti_2AlC and Ti_3AlC_2 Particles-Containing Lubricant under Cyclic Impact Loading

Yan Shen ^{*}, Zhixiang Liu , Chuanfei Xing, Qi Li and Junjing Fan

Key Laboratory of Ship-Machinery Maintenance & Manufacture, Dalian Maritime University, Dalian 116026, China; liuzx@dmlu.edu.cn (Z.L.); xingchaunfei@dmlu.edu.cn (C.X.); li.qi@dmlu.edu.cn (Q.L.); fan@dmlu.edu.cn (J.F.)

* Correspondence: shenyan@dmlu.edu.cn

Abstract: $M_{n+1}AX_n$ (MAX) phase materials present an attractive potential for friction reduction and wear resistance applications due to the ternary layered structure. This work was done to investigate how the combination of Ti_2AlC and Ti_3AlC_2 MAX phase particles with zinc dialkyl dithiophosph (ZDDP) additives in the lubricant affected the tribo-surface by means of a reciprocating test rig with cyclic impact loading. The results indicated that the friction and wear properties of Ti_3AlC_2 -containing lubricant were better than those of Ti_2AlC -containing lubricant. The distinctive microstructure of worn surface caused by the Ti_3AlC_2 particles was characterized by the uniform distribution of many fine scratches, while the other was distributed with more peeling pits by the Ti_2AlC particles. The tribo-chemical reaction of ZDDP involving Ti_3AlC_2 particles promoted a larger regional distribution of the tribofilm and the generation of short-chain phosphates. The synergistic effect of Ti_3AlC_2 particles and ZDDP additives led to excellent tribological properties.

Keywords: friction and wear; MAX phase particle; microstructure; tribofilm



Citation: Shen, Y.; Liu, Z.; Xing, C.; Li, Q.; Fan, J. Tribo-Surface Variation Caused by Ti_2AlC and Ti_3AlC_2 Particles-Containing Lubricant under Cyclic Impact Loading. *Lubricants* **2022**, *10*, 33. <https://doi.org/10.3390/lubricants10030033>

Received: 22 December 2021

Accepted: 21 February 2022

Published: 23 February 2022

Publisher's Note: MDPI stays neutral with regard to jurisdictional claims in published maps and institutional affiliations.



Copyright: © 2022 by the authors. Licensee MDPI, Basel, Switzerland. This article is an open access article distributed under the terms and conditions of the Creative Commons Attribution (CC BY) license (<https://creativecommons.org/licenses/by/4.0/>).

1. Introduction

$M_{n+1}AX_n$ (MAX) phase materials are a group of ternary compounds, where M represents an early transition metal (such as Ti or Nb), A mostly represents a IIIA and IVA group element (such as Al or Si), and X is either carbon or nitrogen [1,2]. MAX phase materials have generated many attractive application scenarios due to their high thermal conductivity, thermal shock resistance, oxidation resistance, etc. [3–6]. Ti_2AlC and Ti_3AlC_2 are typical representatives of MAX phase materials. Their ternary nanolayer compounds with the layered structures may contribute to the development of self-lubricating properties and offer great potential in tribology applications, especially as lubricant additives added into the lubricating oil.

When a portion of the particles are brought into the contacting area of tribo-couple by the lubricant, these particles then produce different mechanisms of action on the worn surface [7]. Some of the particles adhered to the sliding surface, providing the effective lubricating film thickness, and thus avoiding direct contact of micro-asperities [8]. Additionally, the original sliding friction was converted to the sliding friction plus rolling friction [9,10]. Some of the particles flattened the micro-topography through filling and/or polishing the tribological surface, thus facilitating the spreading and distribution of the fluid lubricant film [11]. Some of the particles were involved in the tribo-chemical reactions and formed a layer of chemical reaction film, which served to reduce shear strength, repair surface defects, etc. [12–15]. These mechanisms might act simultaneously or exist alone. Despite many views about the mechanism of action by the particles, the lubrication mechanism of Ti_2AlC and Ti_3AlC_2 particles remains unclear.

At extreme pressure conditions, zinc dialkyl dithiophosphates (ZDDP) additives generally develop the tribo-chemical reaction film in response to the heat and/or stress concentration [16,17]. When the ZDDP additives and the particles contained in the lubricating

oil are delivered to the tribo-surface, the tribo-chemical reaction will be necessarily affected by the particles. Nehme and Dib demonstrated that a tightly bound fluorocarbon and metal fluoride material was formed on the metal surface for ZDDP oils containing FeF_3 +PTFE blends, enhancing wear protection and reducing surface tension [18]. Varlot et al. proposed that tribo-chemical interactions between ZDDP and micellar calcium borate occurred with the formation of a calcium and zinc borophosphate glass tribofilm [19]. Aldana et al. showed that a 50–60 nm tribofilm was formed by the synergetic action between WS_2 fullerene-like nanoparticles and ZDDP additives [20]. Sharma et al. observed that TiO_2 nanoparticles coated with boron-rich plasma films showed good anti-wear performance when used with 350 ppm of ZDDP in the oil [21]. Berkani et al. identified that goethite microparticles in the dispersion led to the formation of a depolymerized zinc-iron phosphate tribofilm [22]. Vyavhare et al. presented that an additive mixture of fluorinated ZnO and ZDDP exhibited a reduction in the coefficient of friction and significantly improved wear performance [23]. In addition, some particles displayed better lubricating performance, showing a trend that might replace or assist ZDDP additives [24–28]. From the above analysis, it is clear that different particles produce different lubrication mechanisms. Regarding Ti_2AlC and Ti_3AlC_2 particles added into ZDDP oil, it still needed to explore these layered structured particles' effect on the impact of friction and wear performance and clarify the tribo-mechanism of such particles under the action of ZDDP.

In this paper, Ti_2AlC and Ti_3AlC_2 particles were separately added into the ZDDP-containing lubricating oil. Friction and wear properties of lubricants containing these two different particles were compared through a reciprocating test rig of cyclic impact loading. The worn surface morphology and tribo-chemical reaction films were analyzed to explore the interaction mechanism between ZDDP and titanium aluminum carbide particles. This exploration may provide some insight into the design of lubricant additives using Ti_2AlC and Ti_3AlC_2 particles.

2. Experimental Details

2.1. Experimental Materials

Both Ti_2AlC and Ti_3AlC_2 were purchased from Zhongxin New Materials Co., Ltd., China. Figure 1 shows the SEM images of the two layered particles. The length-width sizes of both irregular flat-shaped particles are approximately 10 μm with the average thickness of 1–2 μm . It can be seen that the laminar structure was mixed with some small pieces of particles. The crystal structure of Ti_2AlC and Ti_3AlC_2 was further confirmed by XRD analysis, as shown in Figure 2. Both Ti_3AlC_2 and Ti_2AlC were pure phase particles, and no intermediate phase was observed. Each particle was added separately to the lubricating oil at a concentration of 0.33 wt%. In order to use the selected particles in a real engine, engine oil 10 W-40 CF-4 was purchased from the Great Wall Lubricant Corporation of China. It contained approximately 1 wt% of ZDDP additive. It had a viscosity index of 139 and a kinematic viscosity of 103.7 mm^2/s at 40 °C and 13.9 mm^2/s at 100 °C.

Although the engine oil was selected from the perspective of the actual application of the engine, engine oil was initially formulated to the additive already present in the oil. This might bring some concerns due to the miscibility of MAX particles in the engine oil. Therefore, the dispersant oleic acid was used to stabilize the mixture of engine oil and MAX particles. The amount of oleic acid added in the oil sample was 0.5 wt% of the oil. Base oil HVI H5 containing the dispersant oleic acid was also selected to verify the differences in friction and wear performance between the Ti_2AlC and Ti_3AlC_2 particles.

To maintain the stability of particle suspension in the oil sample prior to friction and wear tests, the oil samples were prepared by the steps of magnetic stirring of oleic acid, probe sonicating, and ultrasonic vibrating of the particles [29]. First, the particle and oleic acid solution samples were mixed in lubricant for 3 h using a magnetic stirrer at room temperature. Then, the mixture was homogenized for 4 h using a probe sonicator with a power output of 93 W, a frequency of 19.66 kHz, and a 60% amplitude. Finally, the mixture

was ultrasonically vibrated at 120 W and 40 kHz for 3 h. This could minimize the effect of particle settling on experimental results in friction and wear tests.

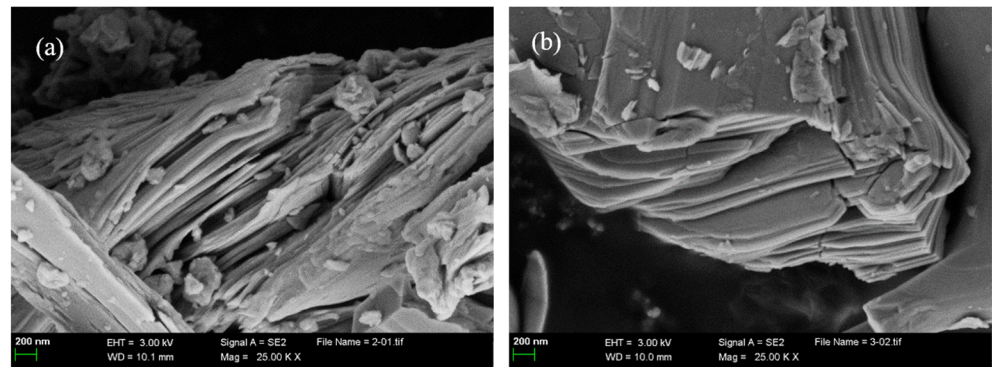


Figure 1. SEM images of Ti_2AlC (a) and Ti_3AlC_2 (b) particles with laminar structure.

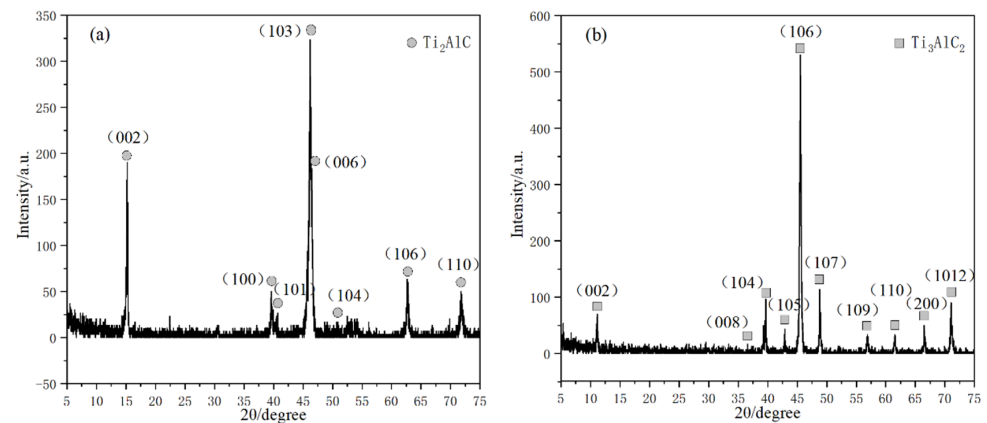


Figure 2. The XRD patterns of Ti_2AlC (a) and Ti_3AlC_2 (b) particles.

In order to reduce testing errors and ensure consistency in the condition of the tested materials, piston ring and cylinder liner used in real engines were chosen as the original tribo-couple to distinguish the tribological behavior of lubricants containing different particles. The difference in tribo-behavior between Ti_2AlC and Ti_3AlC_2 particles can be obtained through a series of repetitive friction and wear experiments. Cast iron cylinder liners with a honing surface were supplied by Yantai Vast Co., Ltd., China. The cylinder liner with an inner diameter of 110 mm was uniformly cut into samples with a length of 43 mm and a thickness of 10 mm. Piston rings with chromium-based ceramic composite coating (CKS) were purchased from Shuang Huan Piston Ring CO., LTD., China. The commercial piston ring with an inner diameter of 70 mm, an outer diameter of 110 mm, and a thickness of 3 mm was cut into 20 samples along the circumference. In order to weaken the influence of hoop stress on wear test, only piston ring samples taken from the opposite side of the gap clearance were used.

2.2. Friction and Wear Tests

Friction and wear tests were performed as reported earlier using a piston ring reciprocating cylinder liner test rig which can simulate the cyclic impacts of peak cylinder pressure [30,31]. The experimental conditions are shown in Table 1. For each test, the speed was set at 200 r/min, corresponding to a reciprocating frequency of 6.67 Hz. The lubricating oil was supplied along a 30 mm stroke at a dosage of 0.1 mL/min. The testing started with a low load in a running-in regime. Afterwards, it increased the load and ran the test for 180 min. The maximum nominal pressure 50 MPa in the steady state corresponded to 1275 N. The temperature was set at 200 °C. These experimental conditions were suitably

enhanced to simulate the friction and wear behavior of a piston ring and cylinder liner at the top dead center in a marine diesel engine.

Table 1. Experimental conditions in friction and wear tests.

Experimental Stage	Experimental Parameters				
	Speed (r/min)	Max. Impact Load (MPa)	Temperature (°C)	Oil Supply Rate (mL/min)	Time (min)
Running in	200	10	200	0.1	10
Steady state	200	50	200	0.1	180

As the applied normal force between the tribo-couple was known, the coefficient of friction at the dead center was calculated from the ratio of the largest friction force to the normal force. The wear depth measured by an OLYMPUS LEXT OLS 3100 optical microscope (Olympus Corporation, Tokyo, Japan) was used to characterize the wear loss of the tribo-couple. The wear depth of the sample was obtained by measuring the height difference of the worn and unworn surfaces. At least three repetitive experiments were carried out under the same test conditions to obtain the coefficient of friction and wear depth. The average values and its standard deviation were calculated from three valid results.

The crystal structures of the particles were analyzed using X-ray diffraction (XRD, D/Max-Ultima⁺, Rigaku, Japan). The worn surfaces were examined using a SUPRA 55 SAPHIRE scanning electron microscope (SEM, Carl Zeiss NTS GmbH, Oberkochen, Germany) and energy dispersive X-ray spectroscopy (EDS, Carl Zeiss NTS GmbH, Oberkochen, Germany). The instrument for detecting and analyzing the chemical composition of the worn surface was a K-Alpha 1063 X-ray photoelectron spectroscope (XPS, Thermo Fisher Scientific, Waltham, MA, USA). The X-ray source was a monochromatic Al K α (1486.6 eV) beam, run at 72 watts. The analyzed area was approximately 400 μm \times 300 μm . Spectral data processing was performed using the Avantage program with the subtraction of a Smart-type background and mixed Gaussian-Lorentzian peaks, with 30% Lorentzian character (GL (30)), fitted to the raw data. After fitting the data, the x -axis of all spectra was charge-calibrated to the C–C component in the C1s fit at 284.8 eV.

3. Results and Discussion

3.1. Comparison of Friction and Wear Performance

Figure 3 shows the variation of friction force throughout the stroke during the stable wear stage. In Figure 3a, the friction force of the lubricating oil containing Ti₂AlC particles was slightly higher than that of the lubricating oil without particles in the middle stroke, but the difference in friction force increased significantly at the dead center. For the lubricating oil containing Ti₃AlC₂ particles, the friction force was clearly the lowest. It exhibited a friction-reducing effect in the entire stroke. As a comparison, the magnitude of the friction force did not vary in the ranking order among base oil containing particles. However, the differences in friction force among base oil containing particles was significantly smaller than the differences among engine oil containing particles in the whole stroke, as shown in Figure 3b.

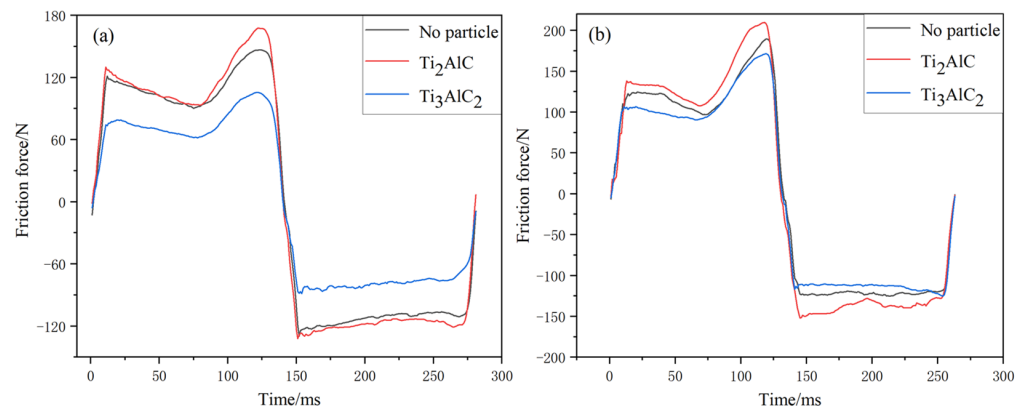


Figure 3. Friction force variation of engine oil (a) and base oil (b) without particles and with Ti_2AlC and Ti_3AlC_2 particles at a temperature of $200\text{ }^{\circ}C$ with maximum impact load of 50 MPa and rotation speed of 200 rpm for a 180 min test duration.

As the sliding speed gradually decreased to zero, the dead center became the location where friction force was highest and wear loss was most likely to occur. Figure 4 shows the comparison of the coefficient of friction and wear depth at the dead center for different compositions of lubricants. Coefficient of friction was taken from the stable wear stage, as shown in Figure 4a. It can be seen that coefficient of friction of the lubricant without particles was about 0.115. The coefficients of friction of lubricants containing Ti_2AlC and Ti_3AlC_2 particles were about 0.133 and 0.084, respectively. The coefficient of friction of lubricants containing Ti_3AlC_2 particles was 27.0% lower than that of the lubricant without particles, while the coefficient of friction of lubricants containing Ti_2AlC particles was 15.7% higher than that of the lubricant without particles. For the lubricant without particles, the wear depth of the cast iron was about $1.73\text{ }\mu m$ but increased to about $1.92\text{ }\mu m$ for Ti_2AlC particles and decreased to about $1.62\text{ }\mu m$ for Ti_3AlC_2 particles (Figure 4b). The variation trend of CKS wear depth was similar to that of the cylinder liner. These results indicate that Ti_3AlC_2 particles improved the friction and wear performance of cast iron/CKS, but Ti_2AlC particles were not good friction modifiers. For the base oil containing particles in Figure 5, the coefficient of friction and wear depth were much larger. There was no essential effect on the ranking order. The friction and wear performance of base oil containing Ti_3AlC_2 particles were still better than those of base oil containing Ti_2AlC particles. Thus, the following analysis focused on a worn surface lubricated by engine oil containing particles.

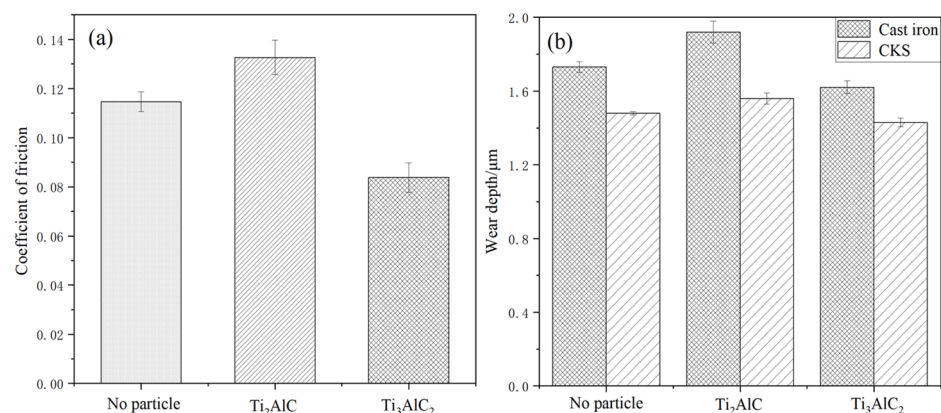


Figure 4. Coefficient of friction (a) and wear depth (b) of engine oil without particles and with Ti_2AlC and Ti_3AlC_2 particles at a temperature of $200\text{ }^{\circ}C$ with maximum impact load of 50 MPa and rotation speed of 200 rpm for a 180 min test duration.

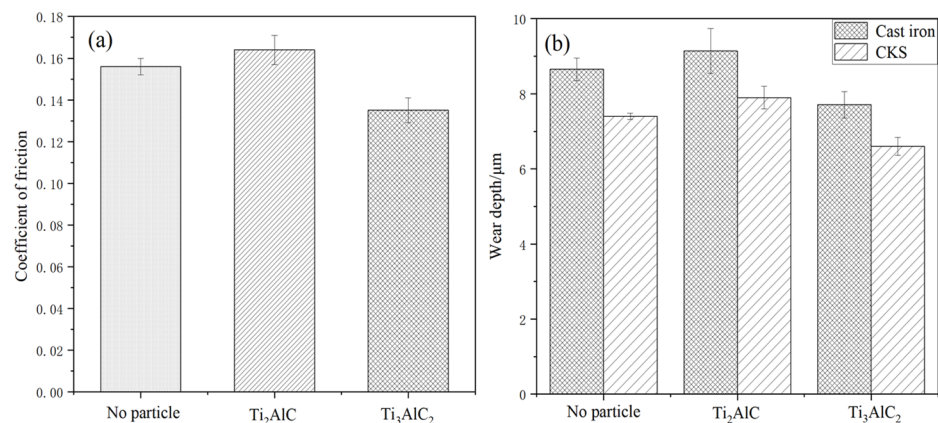


Figure 5. Coefficient of friction (a) and wear depth (b) of base oil without particles and with Ti₂AlC and Ti₃AlC₂ particles at a temperature of 200 °C with maximum impact load of 50 MPa and rotation speed of 200 rpm for a 180 min test duration.

3.2. Worn Surface Analysis

Figures 6–8 present the worn surface morphology and element distribution of a cylinder liner lubricated with different engine oil samples. The surface lubricated without particles (Figure 6a) was slightly smoother as compared to that lubricated with lubricant containing particles (Figures 7a and 8a). Its honing textures on the cylinder liner surface were no longer clear, only keeping the deeper textured grooves. While the honing textures basically disappeared with the lubricant containing Ti₂AlC particles (Figure 7b), the honing textures were clearly visible with the lubricant containing Ti₃AlC₂ particles (Figure 8b). Along the sliding direction, it was difficult to see scratches on the surface when using lubricant alone. However, there were many fine scratches on the surface in the case of Ti₂AlC particles, while more narrow scratches were distributed on the surface with the Ti₃AlC₂ particles. This may have been due to the different damage mechanisms arising from abrasive wear of Ti₂AlC and Ti₃AlC₂ particles. It seems that Ti₃AlC₂ particles were more likely to slip in the contact area of the cast iron surface than Ti₂AlC particles.

In contrast to the elemental distribution at positions 1 and 3, S, P, and Zn could be detected at position 2 on the cast iron surface lubricated without particles, indicating the generation of a ZDDP tribo-chemical reaction. For the lubricant containing Ti₂AlC particles, P, S, and Zn could be observed in both the platform (position 4, position 6) and the groove (position 5) of the honing surface. This indicated that Ti₂AlC particles may have caused scratching to the ZDDP tribofilm or severe plastic deformation to the surface. For the lubricant containing Ti₃AlC₂ particles, P, S, and Zn from the ZDDP tribo-chemical reaction could be found on the platform of the honing surface (position 7, position 8), but not in the groove (position 9). In addition, Ti and Al from Ti₂AlC (position 6) and Ti₃AlC₂ (position 8) particles could both be found on the platform around the grooves of the honing surface. This demonstrated that the particles were embedded on the cast iron surface.

Figure 9 shows the worn surface morphology and elemental distribution of CKS with different engine oil samples. In Figure 9a, the CKS surface used lubricant alone was scattered with scratches of a certain width along the sliding direction. Other than Cr and C existing inside the scratch (position 10), Fe, S, P, and Zn were also found outside the scratches (position 11). This indicated that some tribo-chemical products may have been transferred from the cast iron to the chromium plating layer. As shown in Figure 9b, the CKS surface with lubricant containing Ti₂AlC particles was distributed with some small scratches of varying lengths along the sliding direction. From the EDS of positions 12 and 13, Al and Ti adhered to the surface of the chrome-based piston ring. S, P, and Zn were basically undetected. Flaking occurred in some locations. Surfaces lubricated without particles had more spalling pits than surfaces lubricated with Ti₂AlC particles. In Figure 9c, Ti₃AlC₂ particles in the lubricant caused many scratches of uniform lengths on the CKS surface.

However, unlike the CKS surfaces lubricated with Ti_2AlC particles, the surface lubricated with Ti_3AlC_2 particles detected P, S, and Zn from the ZDDP tribo-chemical reactive product (positions 14 and 15). Few iron-based materials were present on the surface.

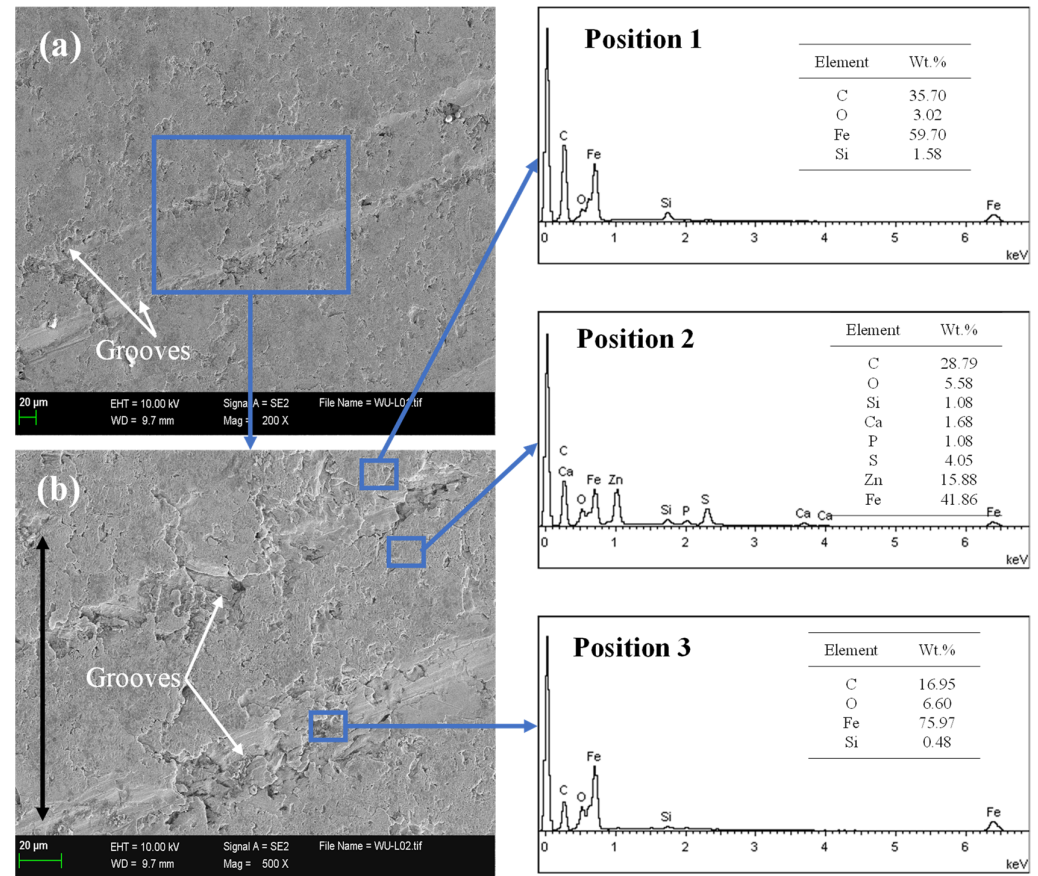


Figure 6. Worn morphology (a), enlarged image (b) and element distribution of a cast iron surface lubricated without particles at a temperature of 200 °C with maximum impact load of 50 MPa and rotation speed of 200 rpm for a 180 min test duration.

3.3. XPS Analysis on Tribofilms of Worn Cast Iron Surface

Peak area ratio, difference between binding energies of the doublets, and full-width at half-maximum (FWHM) were constrained in order to obtain information with the most appropriate chemical meaning [32]. The FWHMs of the peaks constrained to be as equal or as similar as possible for the same element. The signals of phosphorus, sulfur, zinc, titanium, and aluminum of the 2p orbital exhibited two peaks, 2p_{3/2} and 2p_{1/2}, due to spin-orbit splitting with an area ratio of 2:1. The difference in energy was maintained to 0.87 eV for phosphorus, 1.16 eV for sulphur, 23 eV for zinc, 6.0 eV for Al-Ti-C bonds, 5.7 eV for Ti-O bonds, and 0.40 eV for aluminum [33,34].

The detailed spectra of O1s, P2p, S2p, Zn2p, Ti2p, and Al2p recorded on tribofilms formed on the worn surface of cast iron are shown in Figure 10. For P, the P2p_{3/2} peaks appeared around 132.8–133.5 eV (Figure 10(a1–a3)), corresponding to the chemical states of glass-phase phosphates, while the P2p_{3/2} peaks around 134.3 ± 0.1 and 135.5 ± 0.1 eV (Figure 10(a3)) indicated the existence of short-chain phosphates [35]. This could be further verified by the spectra of O1s. Two phosphate-related peaks of NBO (531.9 eV) and BO (533.3 ± 0.3 eV) require special attention [36]. The ratio of BO to NBO, which is closely related to phosphate polymerization, is an important parameter for evaluating phosphate species and their chain lengths [37]. The ratios of lubricated surfaces without particles (Figure 10(b1)) and with Ti_2AlC (Figure 10(b2)) and Ti_3AlC_2 (Figure 10(b3)) particles were 0.27, 0.43, and 0.14, respectively. This was basically in agreement with the states of P2p.

The proportion of short-chain phosphates on the surface lubricated with Ti_3AlC_2 particles was greater than that on the surfaces lubricated with Ti_2AlC particles and without particles. This demonstrated that Ti_3AlC_2 particles promoted the depolymerization process of ZDDP.

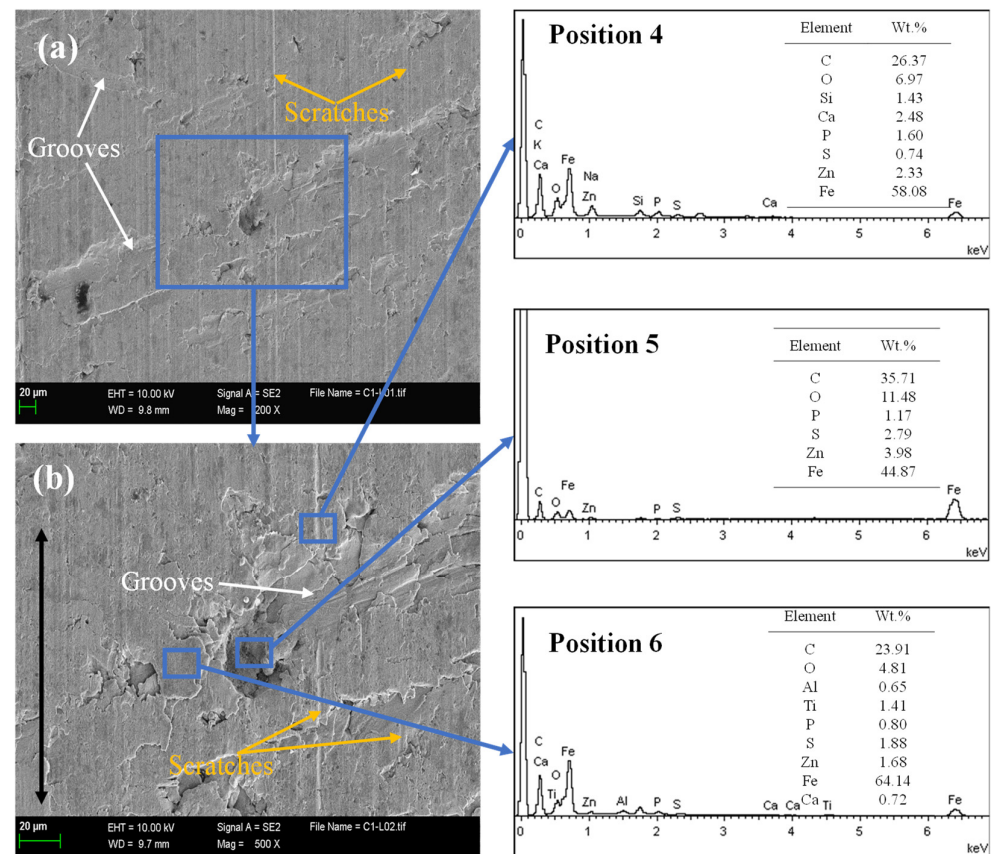


Figure 7. Worn morphology (a), enlarged image (b) and element distribution of cast iron surface lubricated with Ti_2AlC particles at a temperature of 200 °C with maximum impact load of 50 MPa and rotation speed of 200 rpm for a 180 min test duration.

In the case of S, FeS with the binding energy of S2p3/2 at 161.5 ± 0.1 eV was detected in the tribofilms of all three samples (Figure 10(c1–c3)) [32,38]. The S2p3/2 peaks around 168.3 ± 0.3 eV (Figure 10(c1–c3)), corresponding to the chemical states of sulfates [20]. The centered peaks located around 1021.7–1022.0 eV indicated the existence of ZnO (Figure 10(d1–d3)) [38,39]. In addition, other binding energies of Zn2p3/2 around 1023.2 ± 0.2 eV are considered to be zinc phosphate with different chain lengths [40].

For the surface lubricated with the Ti_2AlC particles, the peak located at 458.69 eV of Ti2p3/2 (Figure 10(e1)) indicated the existence of TiO_2 , while Al_2O_3 with the binding energy of Al2p3/2 around 74.6 ± 0.1 eV (Figure 10(f1)) was also detected in the tribofilm [41]. Moreover, the peaks around 454.6 ± 0.1 and 456.4 ± 0.1 eV of Ti 2p3/2 (Figure 10(e1)), 72.2 ± 0.1 eV of Al2p3/2 (Figure 10(f1)) corresponded to the chemical state of the Ti_2AlC particles [42]. The peak distribution of Ti2p (Figure 10(e2)) and Al2p (Figure 10(f2)) on the surface lubricated with Ti_3AlC_2 particles was similar to that on the surface lubricated with Ti_2AlC particles [43]. Although the difference in Ti2p and Al2p peak positions between surfaces lubricated with Ti_2AlC and Ti_3AlC_2 could not be clearly distinguished due to the low content, it still indicated that oxidized (458.8 ± 0.1 eV of Ti2p3/2, 74.2 ± 0.4 eV of Al2p3/2) and unoxidized particles (454.9 ± 0.2 and 456.4 ± 0.1 eV of Ti2p3/2, 72.2 ± 0.1 eV of Al2p3/2) were embedded in the tribofilms of the surface lubricated with Ti_3AlC_2 particles.

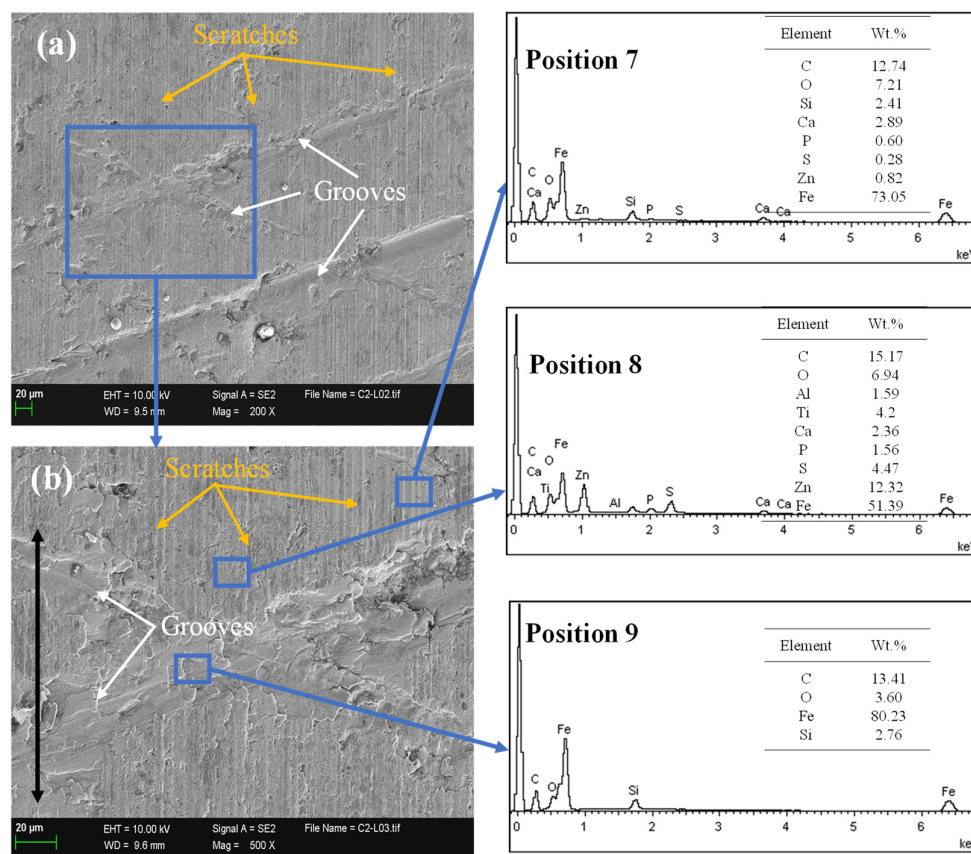


Figure 8. Worn morphology (a), enlarged image (b) and element distribution of cast iron surface lubricated with Ti_3AlC_2 particles at a temperature of 200 °C with maximum impact load of 50 MPa and rotation speed of 200 rpm for a 180 min test duration.

3.4. Lubrication Mechanism Analysis of Lubricants Containing Ti_2AlC and Ti_3AlC_2 Particles

Through a series of friction and wear tests, it was shown that lubricants containing Ti_3AlC_2 particles had better friction reduction and anti-wear performance than those containing Ti_2AlC particles for the cast iron/CKS pair.

Observing the surface of CKS and cast iron, Ti_2AlC particles not only underwent material transfer to the cast iron/CKS surface, but also spalled the surface with the formation of pits (Figures 7b and 9b). However, for the surface lubricated with Ti_3AlC_2 particles, many tiny scratches were found to be evenly distributed like the sliding tracks of a train (Figures 8b and 9c). These fine parallel sliding textures created by the Ti_3AlC_2 particles as well as the presence of honing textures might help to facilitate the distribution of liquid lubricating oil, providing the passages for the directional delivery of lubricants to the contacting interface [44].

Through the EDS measurement, S, P, and Zn were detected on the cast iron surface lubricated with Ti_2AlC particles, but these elements were rarely distributed on the CKS surface. For the Ti_3AlC_2 particles, larger distribution of S, P, and Zn were detected both on the cast iron and the CKS surface. This demonstrated that the tribo-surface structure formed between ZDDP additives, and the sliding surfaces adapted to the sliding conditions with cyclic impact loading [45]. Compared with Ti_2AlC particles, Ti_3AlC_2 particles promoted a larger regional distribution of the tribofilm and more tribo-chemical reactions of ZDDP. XPS analysis demonstrated that the tribofilms had more short-chain phosphates on the surface lubricated with Ti_3AlC_2 particles than that on the surface lubricated with Ti_2AlC particles.

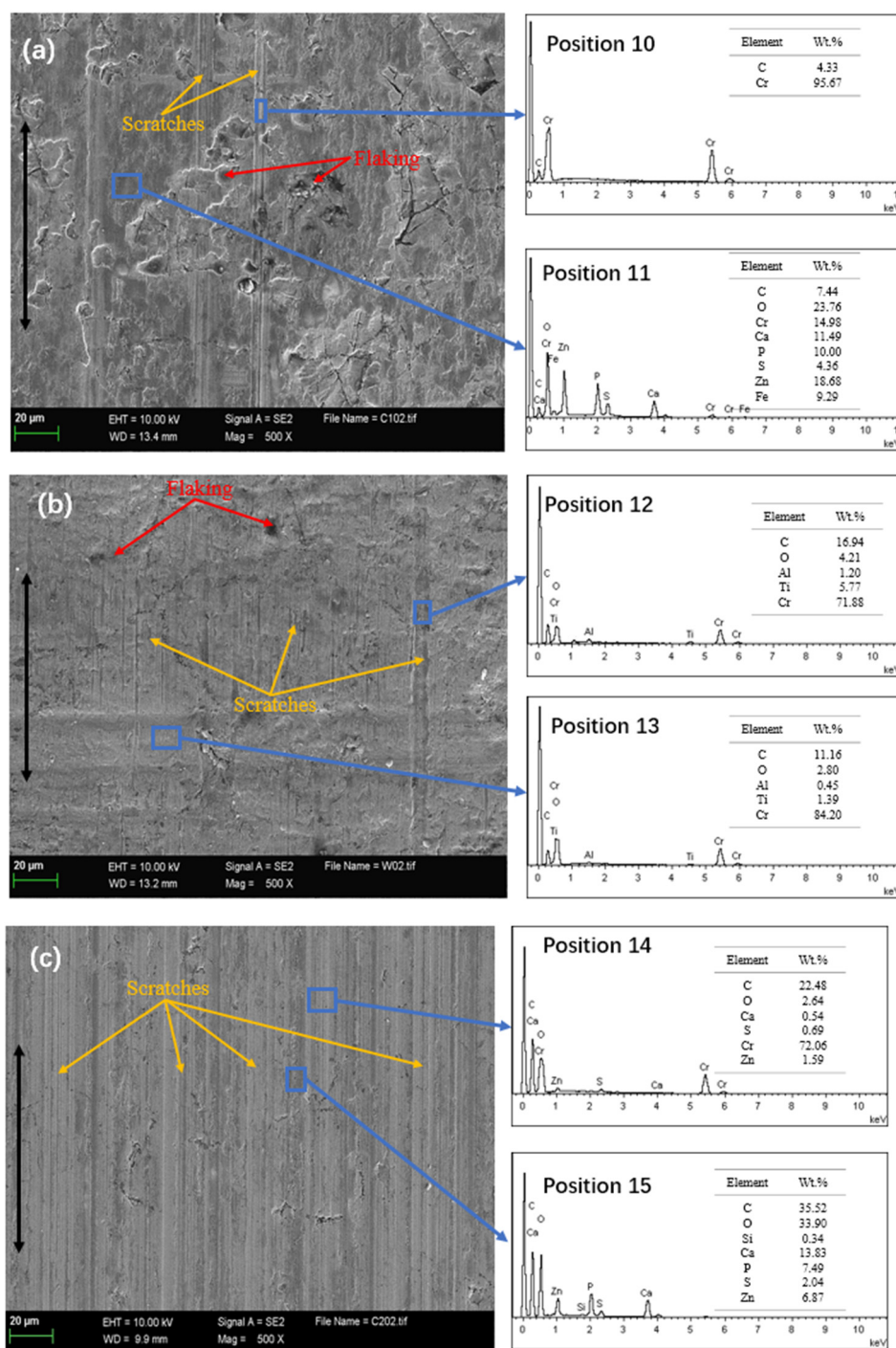


Figure 9. Worn morphology and element distribution of a CKS surface lubricated without particles (a) and with Ti_2AlC (b) and Ti_3AlC_2 (c) particles at a temperature of 200 °C with maximum impact load of 50 MPa and rotation speed of 200 rpm for a 180 min test duration.

Based on the above analysis, the lubricating mechanism of lubricants containing Ti_2AlC and Ti_3AlC_2 particles is shown in Figure 11. Compared with the surface lubricated with Ti_2AlC particles, evenly distributed sliding textures could achieve the directional flow of lubricants and promoted the tribo-chemical reaction of ZDDP on the cast iron/CKS surface lubricated with Ti_3AlC_2 particles. In addition, the tribofilms were present together on the surfaces of CKS and cast iron, avoiding the direct large-area contact between the surface micro-asperities and between the micro-asperities and Ti_3AlC_2 particles without causing serious damage. These mechanical and tribo-chemical interactions generated good

synergistic relation among lubricating oil, ZDDP additives, and Ti_3AlC_2 particles on the cast iron/CKS surface.

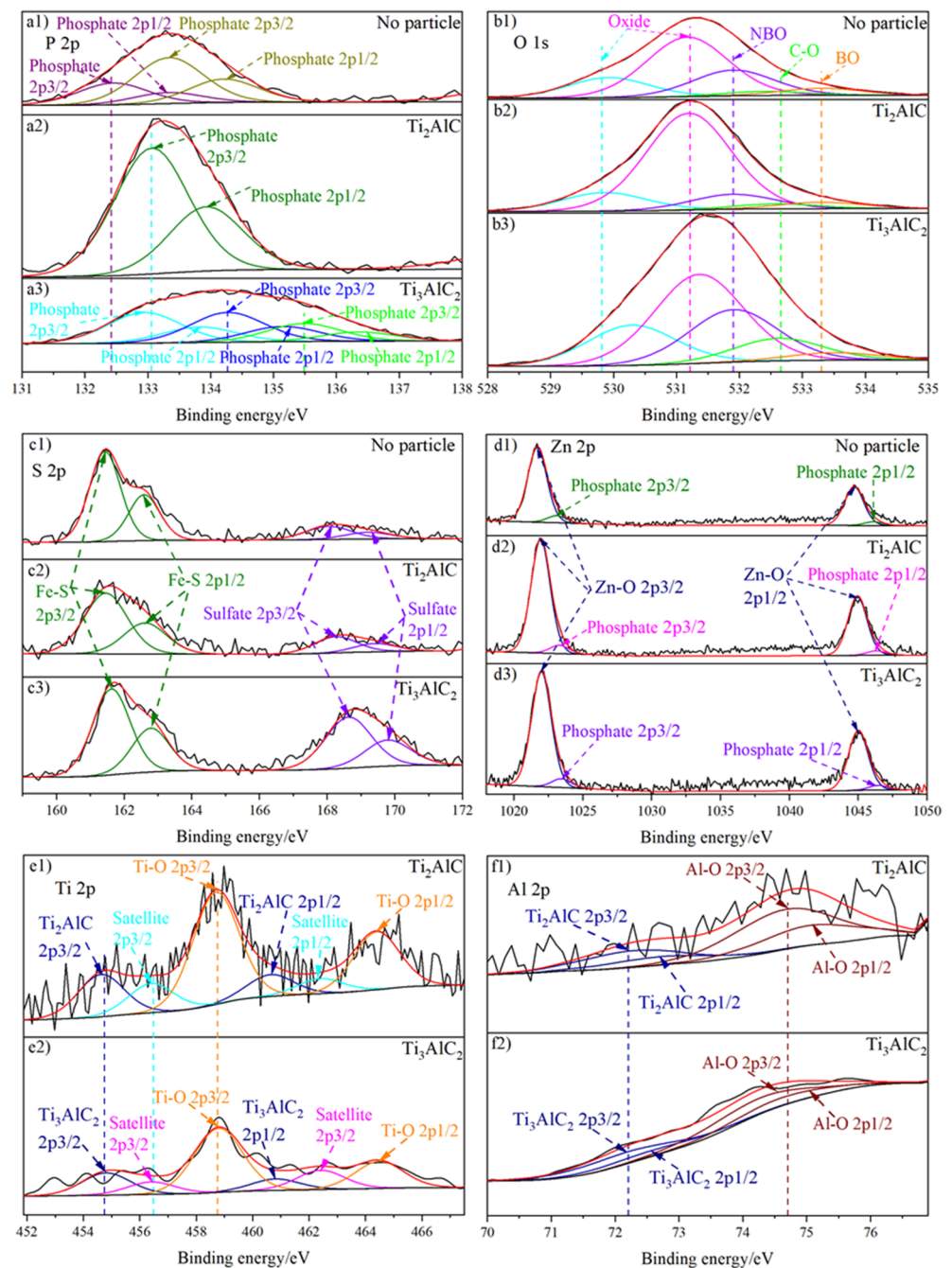


Figure 10. Deconvoluted spectra of P2p (a), O1s (b), S2p (c), Zn2p (d), Ti2p (e), and Al2p (f) peaks recorded on tribofilms of a cast iron surface lubricated without particles and with Ti_2AlC and Ti_3AlC_2 particles at a temperature of 200 °C with maximum impact load of 50 Mpa and rotation speed of 200 rpm for a 180 min test duration.

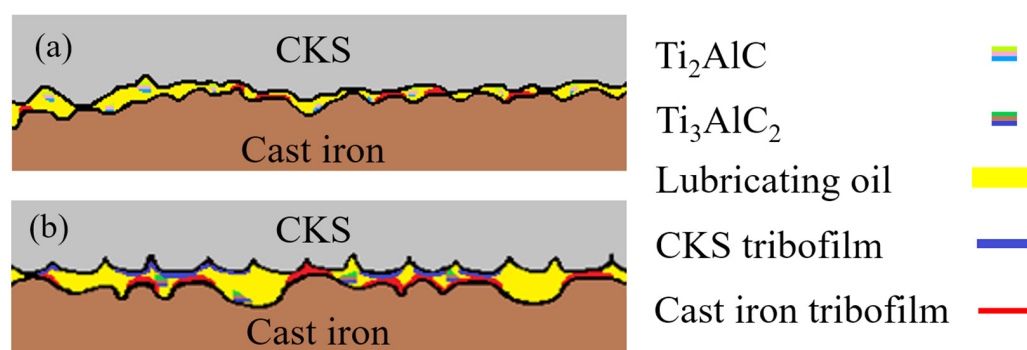


Figure 11. Schematic diagram of lubrication mechanism for the cast iron/CKS surface lubricated with Ti_2AlC (a) and Ti_3AlC_2 (b) particles.

4. Conclusions

At a maximum cyclic impact load of 50 MPa, Ti_2AlC and Ti_3AlC_2 particles presented different tribological behaviors for the ZDDP-containing lubricant and generated different microstructures on the cast iron/CKS surface at a temperature of 200 °C and a speed of 200 r/min. Compared with Ti_2AlC particles, Ti_3AlC_2 particles seemed to be good modifiers for lubricants in terms of friction reduction and wear resistance at the strengthened conditions. The ZDDP additives and Ti_3AlC_2 particles contained in the lubricant could achieve larger region existence of tribofilms on the cast iron/CKS surface with a uniform sliding texture distribution. In addition to FeS, ZnO, TiO_2 , Al_2O_3 , and unoxidized particles detected in the tribofilm, short-chain phosphates were present in a larger proportion on the cast iron surface lubricated with Ti_3AlC_2 particles. Future work should consider more experimental conditions (mainly in terms of loads and speeds) on the effect of Ti_2AlC and Ti_3AlC_2 particles and further verify the differences at different lubricating conditions.

Author Contributions: Y.S.: conceptualization, formal analysis, investigation, methodology, supervision, writing—original draft, writing—review and editing. Z.L.: formal analysis, investigation, writing—original draft, writing—review and editing. C.X.: formal analysis, investigation. Q.L.: investigation. J.F.: methodology. All authors have read and agreed to the published version of the manuscript.

Funding: This work was supported by the National Natural Science Foundation of China (51979018) and the Fundamental Research Funds for the Central Universities (3132019366).

Data Availability Statement: The data presented in this study are available on request from the corresponding author.

Conflicts of Interest: The authors declare no conflict of interests.

References

1. Barsoum, M.W. The $\text{M}_{n+1}\text{AX}_n$ phases: A new class of solids; Thermodynamically stable nanolaminates. *Prog. Solid State Chem.* **2000**, *28*, 201–281. [[CrossRef](#)]
2. Sun, Z. Progress in research and development on MAX phases: A family of layered ternary compounds. *Int. Mater. Rev.* **2011**, *56*, 143–166. [[CrossRef](#)]
3. Li, X.; Xie, X.; Gonzalez-Juliana, J.; Malzbendera, J.; Yang, R. Mechanical and oxidation behavior of textured Ti_2AlC and Ti_3AlC_2 MAX phase materials. *J. Eur. Ceram. Soc.* **2020**, *40*, 5258–5271. [[CrossRef](#)]
4. Sun, G.Q.; Feng, M.; Zhang, K.; Wang, T.H.; Li, Y.H.; Han, D.H.; Li, Y.G.; Song, F. Q-Switched and Mode-Locked Er-doped fiber laser based on MAX phase Ti_2AlC saturable absorber. *Results Phys.* **2021**, *26*, 104451. [[CrossRef](#)]
5. Lu, S.; Li, X.; Zhou, Y.; Xu, W.; Pan, J. Synthesis and mechanical properties of $\text{TiB}_2/\text{Ti}_2\text{AlN}$ composites fabricated by hot pressing sintering. *J. Ceram. Soc. Jan.* **2018**, *126*, 900–905. [[CrossRef](#)]
6. Gonzalez-Julian, J. Processing of MAX phases: From synthesis to applications. *J. Am. Ceram. Soc.* **2021**, *104*, 659–690. [[CrossRef](#)]
7. Tang, Z.; Li, S. A review of recent developments of friction modifiers for liquid lubricants (2007–present). *Curr. Opin. Solid State Mater. Sci.* **2014**, *18*, 119–139. [[CrossRef](#)]
8. Gunda, R.K.; Narala, S.K.R. Tribological studies to analyze the effect of solid lubricant particle size on friction and wear behaviour of Ti-6Al-4V alloy. *Surf. Coat. Technol.* **2016**, *308*, 203–212. [[CrossRef](#)]

9. Wu, Y.; Tsui, W.C.; Liu, T. Experimental analysis of tribological properties of lubricating oils with nanoparticle additives. *Wear* **2007**, *262*, 819–825. [[CrossRef](#)]
10. Chinas-Castillo, F.; Spikes, H.A. Mechanism of action of colloidal solid dispersions. *J. Tribol.* **2003**, *125*, 552–557. [[CrossRef](#)]
11. Lee, K.; Hwang, Y.; Cheong, S.; Choi, Y.; Kwon, L.; Lee, J.; Kim, S.H. Understanding the Role of Nanoparticles in Nano-Oil Lubrication. *Tribol. Lett.* **2009**, *35*, 127–131. [[CrossRef](#)]
12. Hu, Z.; Lai, R.; Lou, F.; Wang, L.; Chen, Z.; Chen, G.; Dong, J. Preparation and tribological properties of nanometer magnesium borate as lubricating oil additive. *Wear* **2002**, *252*, 370–374. [[CrossRef](#)]
13. Zhou, X.; Shi, H.; Zhang, S.; Fu, X.; Wang, X. Friction and Wear Properties of Cyanex 302-Modified MoS₂ Micro-Sized Spheres as Additive in Liquid Paraffin. *Tribol. Trans.* **2008**, *51*, 454–459. [[CrossRef](#)]
14. Liu, G.; Li, X.; Qin, B.; Xing, D.; Guo, Y.; Fan, R. Investigation of the mending effect and mechanism of copper nano-particles on a tribologically stressed surface. *Tribol. Lett.* **2004**, *17*, 961–966. [[CrossRef](#)]
15. Wang, N.; Wang, H.; Ren, J.; Gao, G.; Zhao, G.; Yang, Y.; Wang, J. High-efficient and environmental-friendly PTFE@SiO₂ core-shell additive with excellent AW/EP properties in PAO6. *Tribol. Int.* **2021**, *158*, 106930. [[CrossRef](#)]
16. Gosvami, N.N.; Bares, J.A.; Mangolini, F.; Konicek, A.R.; Yablon, D.G.; Carpick, R.W. Mechanisms of antiwear tribofilm growth revealed in situ by single-asperity sliding contacts. *Science* **2015**, *348*, 102–106. [[CrossRef](#)]
17. Tysoe, W. On Stress-Induced Tribochemical Reaction Rates. *Tribol. Lett.* **2017**, *65*, 48. [[CrossRef](#)]
18. Nehme, G.; Dib, M. Fluorinated mix in plain ZDDP oil and commercial oil using design of experiment analysis of all interactions and fundamental study of fluorinated mix in plain ZDDP oils under 2 different r/min test cycles and extreme boundary lubrication. *Proc. Inst. Mech. Eng. Part J J. Eng. Tribol.* **2011**, *225*, 193–211. [[CrossRef](#)]
19. Varlot, K.; Martín, J.; Grossiord, C.; Vargiolu, R.; Vacher, B.; Inoue, K. A dual-analysis approach in tribochemistry: Application to ZDDP/calcium borate additive interactions. *Tribol. Lett.* **1999**, *6*, 181–189. [[CrossRef](#)]
20. Aldana, P.U.; Vacher, B.; Le Mogne, T.; Belin, M.; Thiebaut, B.; Dassenoy, F. Action Mechanism of WS₂ Nanoparticles with ZDDP Additive in Boundary Lubrication Regime. *Tribol. Lett.* **2014**, *56*, 249–258. [[CrossRef](#)]
21. Sharma, V.; Timmons, R.B.; Erdemir, A.; Aswath, P.B. Interaction of plasma functionalized TiO₂ nanoparticles and ZDDP on friction and wear under boundary lubrication. *Appl. Surf. Sci.* **2019**, *489*, 372–383. [[CrossRef](#)]
22. Berkani, S.; Dassenoy, F.; Minfray, C.; Belin, M.; Vache, B.; Martin, J.M.; Cardon, H.; Montagna, G.; Reynard, B. Model formation of ZDDP tribofilm from a mixture of zinc metaphosphate and goethite. *Tribol. Int.* **2014**, *79*, 197–203. [[CrossRef](#)]
23. Vyavhare, K.; Timmons, R.B.; Erdemir, A.; Edwards, B.L.; Aswath, P.B. Tribochemistry of fluorinated ZnO nanoparticles and ZDDP lubricated interface and implications for enhanced anti-wear performance at boundary lubricated contacts. *Wear* **2021**, *474–475*, 203717. [[CrossRef](#)]
24. Vyavhare, K.; Timmons, R.B.; Erdemir, A.; Edwards, B.L.; Aswath, P.B. Robust interfacial tribofilms by borate- and poly-mercoated ZnO nanoparticles leading to improved wear protection under a boundary lubrication regime. *Langmuir* **2021**, *37*, 1743–1759. [[CrossRef](#)] [[PubMed](#)]
25. Tu, Z.; Hu, E.; Wang, B.; David, K.D.; Seeger, P.; Moneke, M.; Stengler, R.; Hu, K.; Hu, X. Tribological behaviors of Ni-modified citric acid carbon quantum dot particles as a green additive in polyethylene glycol. *Friction* **2020**, *8*, 182–197. [[CrossRef](#)]
26. Meng, Y.; Su, F.; Chen, Y. Supercritical Fluid Synthesis and Tribological Applications of Silver Nanoparticle-decorated Graphene in Engine Oil Nanofluid. *Sci. Rep.* **2016**, *6*, 31246. [[CrossRef](#)]
27. Zhang, R.; Ding, Q.; Zhang, S.; Niu, Q.; Ye, J.; Hu, L. Construction of a continuously layered structure of h-BN nanosheets in the liquid phase via sonication-induced gelation to achieve low friction and wear. *Nanoscale* **2019**, *11*, 12553–12562. [[CrossRef](#)]
28. Huynh, K.K.; Tieu, K.A.; Pham, S.T. Synergistic and Competitive Effects between Zinc Dialkyldithiophosphates and Modern Generation of Additives in Engine Oil. *Lubricants* **2021**, *9*, 35. [[CrossRef](#)]
29. Ali, M.K.A.; Hou, X. Colloidal stability mechanism of copper nanomaterials modified by bis(2-ethylhexyl) phosphate dispersed in polyalphaolefin oil as green nanolubricants. *J. Colloid Interface Sci.* **2020**, *578*, 24–36. [[CrossRef](#)]
30. Li, W.; Yu, B.; Ye, B.; Shen, Y.; Huang, R.; Du, F. Effects of Cast-Iron Surface Texturing on the Anti-Scuffing Performance under Starved Lubrication. *Materials* **2019**, *12*, 1586. [[CrossRef](#)]
31. Wang, W.; Li, C.; Yang, J.; Shen, Y.; Xu, J. Friction performance of MoDTP and ester-containing lubricants between CKS piston ring and cast iron cylinder liner. *Lubr. Sci.* **2018**, *30*, 33–43. [[CrossRef](#)]
32. Morina, A.; Neville, A.; Priest, M.; Green, J.H. ZDDP and MoDTC interactions and their effect on tribological performance—Tribofilm characteristics and its evolution. *Tribol. Lett.* **2006**, *24*, 243–256. [[CrossRef](#)]
33. Table of Elements. Available online: <https://www.thermofisher.cn/cn/zh/home/materials-science/learning-center/periodic-table.html> (accessed on 25 January 2022).
34. Nslund, L.K.; Persson, P.; Rosen, J. X-ray photoelectron spectroscopy of Ti₃AlC₂, Ti₃C₂T_z, and TiC provides evidence for the electrostatic interaction between laminated layers in MAX-Phase materials. *J. Phys. Chem. C.* **2020**, *124*, 27732–27742. [[CrossRef](#)]
35. Costa, H.L.; Evangelista, K.S.; Cousseau, T.; Acero, J.S.R.; Kessler, F. Use of XANES and XPS to investigate the effects of ethanol contamination on anti-wear ZDDP tribofilms. *Tribol. Int.* **2021**, *159*, 106997. [[CrossRef](#)]
36. Massoud, T.; De Matos, R.P.; Le Mogne, T.; Belin, M.; Cobian, M.; Thiébaut, B.; Loehlé, S.; Dahlem, F.; Minfray, C. Effect of ZDDP on lubrication mechanisms of linear fatty amines under boundary lubrication conditions. *Tribol. Int.* **2020**, *141*, 105954. [[CrossRef](#)]
37. Minfray, C.; Martin, J.M.; Esnouf, C.; Mogne, T.L.; Kersting, R.; Hagenhoff, B. A multi-technique approach of tribofilm characterisation. *Thin Solid Film.* **2004**, *447*, 272–277. [[CrossRef](#)]

38. Nedelcu, I.; Piras, E.; Rossi, A.; Pasaribu, H.R. XPS analysis on the influence of water on the evolution of zinc dialkyldithiophosphate-derived reaction layer in lubricated rolling contacts. *Surf. Interface Anal.* **2012**, *44*, 1219–1224. [[CrossRef](#)]
39. Huai, W.; Chen, X.; Lu, F.; Zhang, C.; Ma, L.; Wen, S. Tribological properties of sulfur- and phosphorus-free organic molybdenum compound as additive in oil. *Tribol. Int.* **2020**, *141*, 105944. [[CrossRef](#)]
40. Crobu, M.; Rossi, A.; Mangolini, F.; Spencer, N.D. Tribochemistry of Bulk Zinc Metaphosphate Glasses. *Tribol. Lett.* **2010**, *39*, 121–134. [[CrossRef](#)]
41. Iatsunskyi, I.; Gottardi, G.; Micheli, V.; Canteri, R.; Coy, E.; Bechelany, M. Atomic layer deposition of palladium coated TiO₂/Si nanopillars: ToF-SIMS, AES and XPS characterization study. *Appl. Surf. Sci.* **2021**, *542*, 148603. [[CrossRef](#)]
42. Wilhelmsson, O.; Palmquist, J.-P.; Lewin, E.; Emmerlich, J.; Eklund, P.; Persson, P.; Högberg, H.; Li, S.; Ahuja, R.; Eriksson, O.; et al. Deposition and characterization of ternary thin films within the Ti–Al–C system by DC magnetron sputtering. *J. Cryst. Growth* **2006**, *291*, 290–300. [[CrossRef](#)]
43. Mahmoudi, Z.; Tabaian, S.H.; Rezaie, H.R.; Mahboubi, F.; Ghazali, M.J. Synthesis of Ti₂AlC & Ti₃AlC₂ MAX phases by Arc-PVD using Ti–Al target in C₂H₂/Ar gas mixture and subsequent annealing. *Ceram. Int.* **2020**, *46*, 4968–4975.
44. Edachery, V.; Shashank, R.; Kailas, S.V. Influence of surface texture directionality and roughness on wettability, sliding angle, contact angle hysteresis, and lubricant entrapment capability. *Tribol. Int.* **2021**, *158*, 106932. [[CrossRef](#)]
45. Wan, S.; Tieu, A.K.; Xia, Y.; Wang, L.; Li, D.; Zhang, G.; Zhu, H.; Tran, B.H.; Mitchell, D. Tribochemistry of adaptive integrated interfaces at boundary lubricated contacts. *Sci. Rep.* **2017**, *7*, 9935. [[CrossRef](#)] [[PubMed](#)]